Arabian Journal of Geosciences (2019) 12:656
https://doi.org/10.1007/s12517-019-4852-8

ORIGINAL PAPER

# Experimental study on the mechanical properties weakening mechanism of siltstone with different water content

Bingyang Li[1,2] · Jian Liu[1,2] · Kang Bian[1,2] · Fei Ai[1,2] · Xunjian Hu[1,2] · Ming Chen[1,2] · Zhenping Liu[1,2]

Received: 18 December 2018 / Accepted: 12 September 2019


## Abstract

The mechanical properties of rock materials are remarkably affected by water content. To reveal the effect of water content on the strength and deformation properties of siltstone, which was collected from the quarry of Zhundong Coalmine, the scanning electron microscope and uniaxial compression tests of siltstone specimens were carried out with a water content of 0%, 0.5%, 1.5%, and 2.8%. Conventional triaxial compression test was conducted in dry and saturated conditions. The test results showed that the strength and deformation parameters of siltstone are weakened with different degrees after water absorption. The deformation of the plastic yield stage in the stress-strain curve decreases with rising of water content, while the loss rate of uniaxial compression strength continues to increase until reached saturated state. The strength of dry and saturated specimens varies regularly with confining pressure, and their relationship can be described with the exponential criterion. In addition, it is observed that microscopic damage of siltstone specimens accumulates as water content increases. The hydration of clay minerals reduces the local cohesion of specimens, and the hydrolysis of quartz minerals in crack tip region promotes subcritical crack growth during the loading process, which collaboratively results in the bearing capacity of saturated specimen decrease. The results can provide a reference for the analysis of rock strength and damage mechanism under the action of water erosion.

**Keywords** Water content · Strength · Confining pressure · Exponential criterion · Microscopic damage

## Introduction

Rock strength is one of the main mechanical properties. Besides the influencing of internal microstructure and mineralogical composition, water is also an important factor affecting the strength (Burshtein 1969; Hawkins and McConnell 1992). The strength of rock will weaken after encountering water, which triggers many engineering problems, such as roadway collapse, slope instability, and tunnel surrounding rock damage (Iverson 2000; Hudson and Harrison 2000; Bian et al. 2019).

The effect of water on the mechanical characteristics of rock materials has been investigated extensively in recent years. Lots of research have shown that the strength may significantly be lowered with a small increase in water content, especially sedimentary rock such as siltstone, sandstone, argillaceous sandstone, and mudstone (Baud et al. 2000; Zhang et al. 2014; Torres-Suareza et al. 2014; Lu et al. 2017). The strength, deformation, and failure characteristics of clay soft rock are closely related to water content. The uniaxial compression strength (UCS), shear strength, and elastic modulus under saturation state are reduced by about 90% compared with dry, much of the strength loss occurred in the range of 0~2% water content (Erguler and Ulusay 2009; Hu et al. 2014; Bian et al. 2019). There is a positive correlation between the effective porosity and water content of sandstone, and its sensitivity to water depends largely on effective porosity (Vásárhelyi and Ván 2006; Wong et al. 2016). Besides, the tensile strength, deformation modulus, and fracture strengths of sandstone decrease when saturation degree increases (Hashiba and Fukui 2015; Roy et al. 2017; Chen et al. 2019). From the microscopic view, the microscopic structural characteristics of the rock, such as the geometry of fissures,

Responsible Editor: Zeynal Abiddin Erguler

✉ Bingyang Li
liby0521@163.com

[1] State Key Laboratory of Geomechanics and Geotechnical Engineering, Institute of Rock and Soil Mechanics, Chinese Academy of Sciences, Wuhan 430071, China

[2] University of Chinese Academy of Science, Beijing 100049, China

Published online: 26 October 2019

the composition of clay minerals, and the contact mode of particles all have a noticeable impact on the strength during the physical and chemical interaction with water (Hadizadeh and Law 1991; Verstrynge et al. 2014; Liu and Cao 2016; Wu et al. 2019).

In addition, the strength and deformation properties of the rock are affected by confining pressure, and its strength increases when confining pressure increases (Haimson 2006; Yang et al. 2012). If the impact of intermediate principal stress on the strength is not considered, the Coulomb criterion and the Hoek-Brown criterion are widely used in rock mechanics research (Hoek 1990; Sofianos and Nomikos 2006; Bagheripour et al. 2011). The strength linearly changes with confining pressure in small stress range, and their relationship can be expressed with the Coulomb criterion. However, experimental studies have shown that the strength rising rate of the cylindrical specimen gradually decreases with confining pressure and the strength is a nonlinear increase (Mogi 2007). The Hoek-Brown criterion is only an empirical equation without a clear physical background and gives a high estimate of experimental data under high confining pressure (You 2011). You M proposed an exponential strength criterion which is considered that cohesion and friction of rock cannot act at the same location simultaneously, and the fitting results of this criterion are better than the existing conventional triaxial strength criteria (You 2010). At present, lots of research results are about the effect of water on UCS, while the mechanical characteristics of siltstone under the confining pressure and water are still inadequate (Chang and Haimson 2007; Li et al. 2012). Therefore, it is necessary to implement the triaxial compression test to obtain more mechanical properties of siltstone.

In this paper, siltstone specimens after water absorption treatment were taken as a research object and a series of experiments were conducted. Scanning electron microscope (SEM) and X-ray diffraction (XRD) tests were carried out to obtain the microstructure features and the mineral composition. In addition, uniaxial and triaxial compression tests were implemented to measure the mechanical parameters of strength and deformation with different water content. According to the results of SEM, the weakening mechanism of siltstone after water absorption was analyzed from the microscopic perspective, which is important for damage analysis of engineering rock strength under the action of water erosion.

## Specimen preparation and testing procedure

The siltstone material used in the study was collected from the quarry of Zhundong Coalmine. It is an open-pit mine and located in the northeast of Xinjiang, China. In order to diminish the scattering due to the anisotropy between the specimens, the core was drilled in the same direction and then cut into a cylindrical specimen with a diameter of 50 mm and a height of 100 mm. According to the rock mechanics standard measurement method, all specimens were polished to make the end surfaces perpendicular to the longitudinal axis within 0.02 mm (ISRM 1978). The specimens were weighed after placing indoors for one week. The natural density of the specimen is in the range of 2179.5~2309.9 kg/m$^3$, the average value is 2239.1 kg/m$^3$, so the specimens are relatively homogeneous.

The rock specimens are shown in Fig. 1. The dry specimens are light gray and its texture is dense. There are no visible defects in the specimen appearance. The specimens turned dark gray and the water became turbid after soaking. When the specimen reached saturation state, its volume expanded by about 1.24%. The siltstone has a weak swelling potential. Figure 1c shows the electron spectroscopy of siltstone.

The mineral compositions of siltstone were measured with an X-ray spectrometer technique and the test results are listed in Table 1. As can be seen from Table 1, this siltstone is mainly composed of quartz (70.7%), albite (11.8%), calcite (2.6%), and clay minerals (14.9%) which are mostly illite and kaolinite. The porosity of siltstone is approximately 6.8%.

At a temperature of 110 °C, the cylindrical specimens were dried for 24 h in the oven. Subsequently, they were divided into 4 groups and the weights of the dried specimens were measured after cooling to ambient temperature. Specimens were treated by the way of natural water absorption to obtain the different water content.

First, they were placed into the container and pure water was injected to 1/4 specimen height. Subsequently, water was injected to 1/2 specimen height and 3/4 specimen height every 2 h, respectively. The specimens were completely submerged after 4 times of water injection according to the standard measurement method (**SL264-2001 2001**). The water content was measured by weight at time intervals of 2 h. After 24 h, the time interval between measurements was increased to 4 h, and a larger interval was later adopted until the weight of the specimen remained unchanged. When specimens were taken out of the water container, their surfaces were coated with paraffin and wrapped with a waterproof membrane in time to prevent water loss.

To reveal the mechanical properties of siltstone in different water content conditions, the uniaxial and conventional triaxial compression tests were implemented in RMT-150C rock mechanics test system. All tests were implemented by displacement control with a constant axial loading rate of 0.002 mm/s. The confining pressure loading rate is 0.1 MPa/s, and the control range of confining pressure is 5–40 MPa.

(a) Dry specimens

(b) Saturated specimens

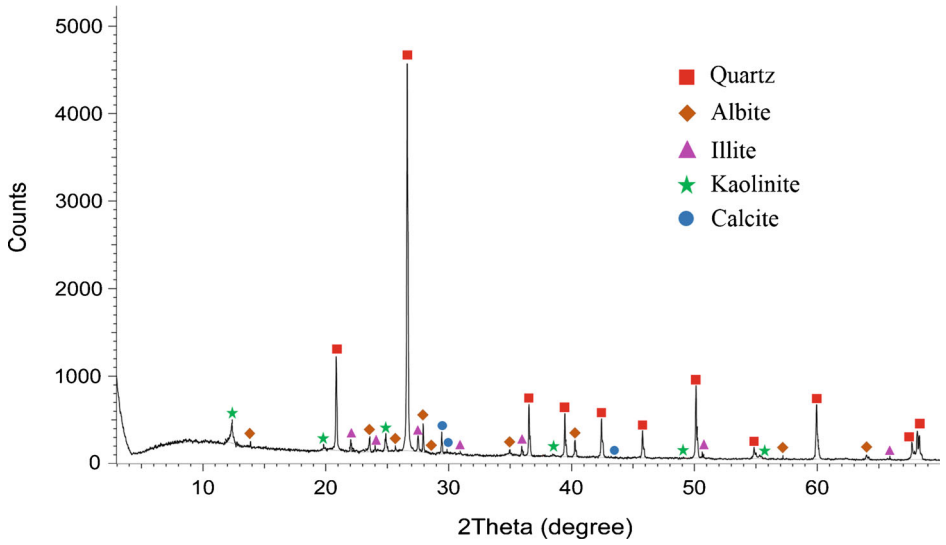


(c) The electron spectroscopy of siltstone.

**Fig. 1** The siltstone specimens and the results of the X-ray diffraction spectrum test

## Experimental results

### Determination of water content

At ambient temperature, the dry specimens were put into the water container, and the water content was determined by the weight increase of the specimen at different times during the natural water-saturated process. Therefore, the water content in the specimen can be defined as follows:

$$w_t = (m_t - m_d)/m_d \times 100\% \quad (1)$$

where $w_t$ is the water content of the specimens after soaking for $t$ hours, $m_t$ and $m_d$ are the mass of wet specimen at soaking time $t$ and dry specimen, respectively.

Figure 2 shows the change of water content with immersion time for three siltstone specimens during the process of saturation. The water content of specimen nonlinearly increases with immersion time and the process is roughly composed of three stages: a rapidly rising stage, a slowly rising stage, and finally saturation. It is consistent with the water absorption process of coal and black sandstone (Yao et al. 2015; Tang 2018). The water content increased rapidly in the first 24 h, which is nearly linear with the water absorption time. Subsequently, the water absorption rate gradually

**Table 1** Mineral content of siltstone specimens

| Composition | Chemical formula | Content (%) |
|---|---|---|
| Quartz | $SiO_2$ | 70.7 |
| Albite | $(Na_{0.98}Ca_{0.02})(Al_{1.02}Si_{2.98}O_8)$ | 11.8 |
| Illite | $2K_2O{\cdot}3MgO{\cdot}Al_2O_3{\cdot}24SiO_2{\cdot}12H_2O$ | 8.7 |
| Kaolinite | $Al_2Si_2O_5(OH)_4$ | 6.2 |
| Calcite | $CaCO_3$ | 2.6 |

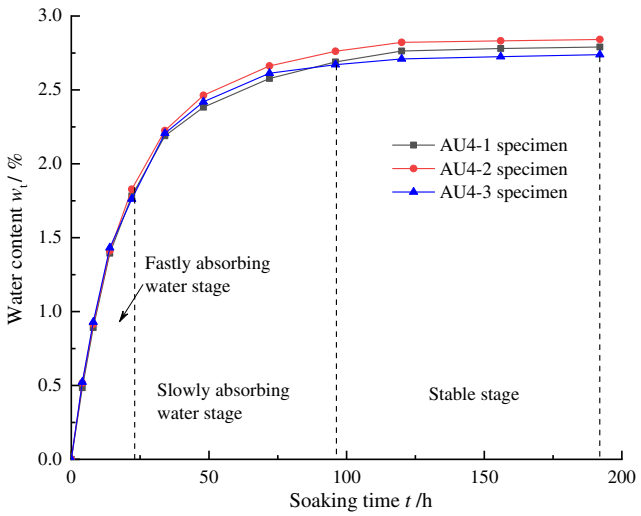


**Fig. 2** Relationship of water content and soaking time for siltstone specimens

decreases, and it is close to saturation after 72 h. Finally, the specimen reaches the water saturation level, and the corresponding water content is approximately 2.8%.

The water content of these three specimens changed consistently with soaking time, indicating that the rock specimen was homogeneous. To better show the weakening of water content on the UCS, we selected four representative water contents of 0%, 0.5%, 1.5%, and 2.8% as the test target, and they are corresponding to a different soaking time which is about 0, 4, 25, and 192 h, respectively.

## Uniaxial compressive test results

### The uniaxial compression stress-strain curve

Figure 3 shows the uniaxial compression stress-strain curves of siltstone in different water content conditions. As shown in this figure, the specimens have experienced microcrack compression, elastic deformation, plastic yield deformation, and post-peak failure stages during the process of compressive deformation. The deformation of the specimen in the plastic yield stage decreases with rising of water content. When the water content exceeds 1.49%, the post-peak stress of specimen falls off quickly and it exhibits brittle fracture characteristic. There are natural fissures in the specimen; the porewater in the specimen is squeezed during the loading process, which results in the porewater pressure increase and the stress concentration at the crack tip region, so the cracks are easier to expand (Zhou et al. 2018). In addition, the UCS, elastic modulus, and peak strain of specimen all decrease when water content increases. The siltstone produced weakened damage after absorbing water and the higher the water content, the more obvious the weakening phenomenon is.

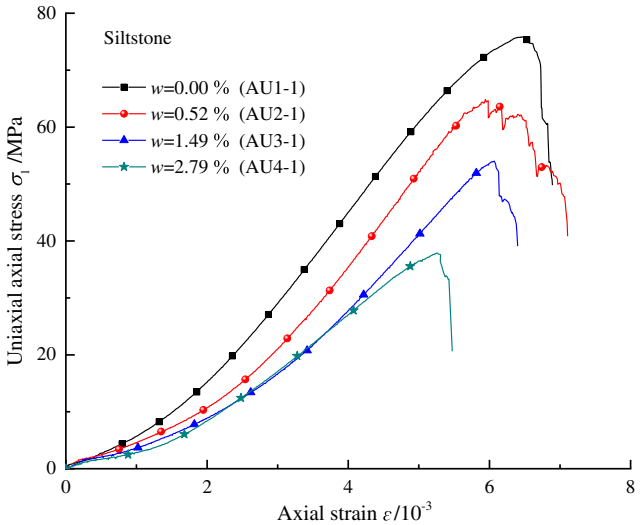


**Fig. 3** The uniaxial compression stress-strain curves with different water content

Table 2 presents the test results of uniaxial compression tests of siltstone. As shown in Table 2, the strength of the specimen has a varying degree of scattering from the test results, which is related to the heterogeneity of the rock. To better show the effect of water content on the UCS, the strength loss rate *K*s is also given in the table at different water content. It is defined as (Wong et al. 2016):

$$K_s = \left(\mathrm{UCS_{dry}} - \mathrm{UCS_w}\right)/\mathrm{UCS_{dry}} \times 100\% \quad (2)$$

where $\mathrm{UCS_{dry}}$ and $\mathrm{UCS_w}$ are the UCS of the dry and wet specimen with water content *w*, respectively.

As shown in Table 2, the UCS of three specimens in the dry condition range from 70.5 to 79.2 MPa, the variation range is 11%, and the average value is 75.2 MPa. The UCS in the saturated condition range from 35.2 to 39.4 MPa, the variation range is 10.7%, and the average value is 37.5 MPa. Comparing the variation range of UCS in these two conditions, the scattering of UCS is not affected by the increase in water content.

### Influence of water content on UCS

Figure 4 shows the UCS and the average value of each group, and the fitting curve of water contents with strength is also given in this figure. In Fig. 4, the UCS gradually decreases when the water content increases. Compared with the dry specimens, the average strength of three saturated specimens is reduced by 50.1%. If the AU4-2 specimen with the highest water content (2.82%) is calculated, the strength loss rate will be greater, indicating that the UCS of siltstone is significantly affected by water content.

The UCS of 12 siltstone specimens varies nonlinearly with water content. It is found that their variation law can be expressed with the following exponential equation (Hawkins and McConnell 1992):

$$\sigma_c(w) = a_0 e^{-bw} + a_1 \quad (3)$$

where $\sigma_c$ is the UCS, *w* is water content, $a_0$, $a_1$, and *b* are constants. When the water content is zero, the compressive strength is $a_0 + a_1$. The parameter *b* is the strength loss rate when the water content increases. As shown in Fig. 4, exponential Eq. (3) can well describe the variation trend of UCS with water content. The best fitting results of the three parameters are $a_0 = 17.71$, $a_1 = 57.44$, and $b = 0.383$. The correlation fit results are given in Table 3.

### Influence of water content on deformation

The test results of elastic modulus and peak strain are given in Fig. 5. As shown in this figure, the peak strain and the elastic modulus gradually decrease with increasing water content. In Fig. 5a, the average value of the elastic modulus of dry specimens is 16.1 GPa and the saturated specimen is 10.6 GPa; the

**Table 2** Physicomechanical parameters of siltstone in uniaxial compression with different water content

| Specimen no. | Density ($\rho$)/kg m$^{-3}$ | Water content ($w$)/% | Peak stress ($\sigma_c$)/MPa | Elastic modluls ($E$)/GPa | Peak strain ($\varepsilon$)/10$^{-3}$ | Strength loss rate ($K_S$)/% |
|---|---|---|---|---|---|---|
| AU1-1 | 2209.6 | 0 | 75.8 | 15.47 | 6.434 | |
| AU1-2 | 2179.5 | 0 | 79.2 | 16.08 | 6.631 | 0 |
| AU1-3 | 2223.2 | 0 | 70.5 | 16.66 | 6.353 | |
| AU2-1 | 2194.6 | 0.517 | 62.2 | 14.45 | 6.002 | |
| AU2-2 | 2231.7 | 0.474 | 67.1 | 13.71 | 6.231 | 13.6 |
| AU2-3 | 2201.4 | 0.526 | 65.4 | 14.83 | 6.258 | |
| AU3-1 | 2281.1 | 1.488 | 53.3 | 10.82 | 5.758 | |
| AU3-2 | 2226.1 | 1.513 | 51.4 | 12.18 | 5.664 | 34.2 |
| AU3-3 | 2246.8 | 1.561 | 43.6 | 11.28 | 5.437 | |
| AU4-1 | 2291.1 | 2.792 | 37.9 | 9.82 | 5.255 | |
| AU4-2 | 2263.2 | 2.824 | 35.2 | 10.99 | 4.526 | 50.1 |
| AU4-3 | 2277.5 | 2.743 | 39.4 | 11.13 | 5.181 | |

elastic modulus loss is about 34.0%. Compared with the UCS loss rate of 50.1% in the two conditions, the water content has a greater weakening effect on the UCS during the plastic deformation stage. This can also be proved in Fig. 3 that when the water content exceeds 1.49%, the stress-strain curve has almost no plastic yielding platform before reaching the peak stress.

The elastic modulus decreases nonlinearly with the increase of water content; it is similar to the variation law of UCS with water content, which can also be described by the exponential Eq. (3).

In Fig. 5b, the average peak strain of dry and saturated specimens are $6.473 \times 10^{-3}$ and $4.987 \times 10^{-3}$, respectively. The peak strain reduction is about 22.9%, while the elastic modulus reduction is about 34.0%, indicating that when the water content is high, the specimen has a small plastic yield deformation before reaching the peak strain and shows more brittle failure characteristics.

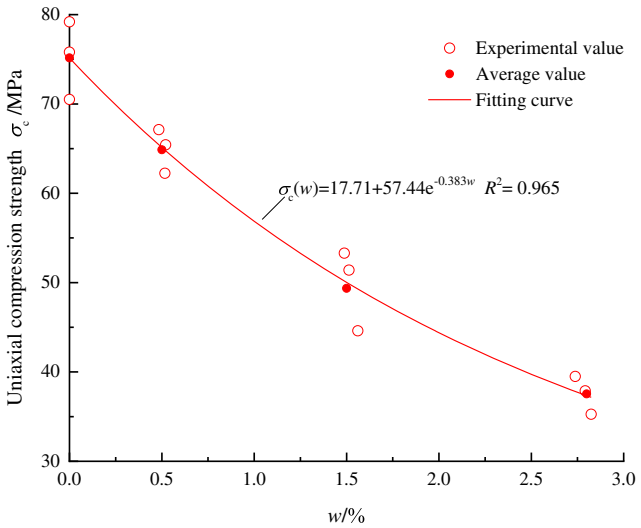


**Fig. 4** Variation of UCS with water content for siltstone specimens

The peak strain varies linearly with water content, and their variation law is different from UCS and elastic modulus. The relationship between water content and peak strain can be expressed with the linear equation:

$$\varepsilon(w) = c\text{-}c_1 w \tag{4}$$

where $c$ and $c_1$ are constants, and $\varepsilon(w)$ is the peak strain. The peak strain of dry specimen is $c$, and $c_1$ is the influence coefficient of the water content on the peak strain. The fitting result of siltstone is $c = 6.444$, $c_1 = 0.528$. The correlation fit results are also listed in Table 3.

## Triaxial compressive test results

### The triaxial compressive stress-strain curve

The conventional triaxial compressive stress-strain curves of siltstone specimens are given in Fig. 6. The mechanical parameters of triaxial tests are presented in Table 4. In Fig. 6, besides the impact of confining pressure, the deformation and strength of siltstone are also affected by the water. In Fig. 6a, the elastic deformation of dry siltstone specimen is obviously increased with the increase in confining pressure, the bearing capacity of the specimen is improved, the plastic yielding platform appears near the peak stress, and the range of the yielding platform is greater when the confining pressure is higher. It indicates that under the high confining pressure, the plastic deformation near the peak stress continues to increase, but the bearing capacity of the specimens no longer increases. This phenomenon can be explained that during the process of plastic yielding, the cohesion of the material is destroyed and converted into frictional bearing capacity, but macroscopic fracture surface is not formed. The increase of deformation can only cause more materials to break, and the

**Table 3** Fitting results of mechanical parameters with the water content

| Mechanical properties | Fitting equation | Correlation coefficient $R^2$ |
|---|---|---|
| UCS | $\sigma_c(w) = 17.71 + 57.44e^{-0.383w}$ | 0.965 |
| Elastic modulus | $E(w) = 9.79 + 6.35e^{-0.796w}$ | 0.936 |
| Peak strain | $\varepsilon(w) = 6.444 - 0.528w$ | 0.998 |

axial stress does not continue to increase. There is residual strength of specimens in the post-peak stage, which mainly depends on the friction between the cracks to bear the load, and it increases when confining pressure increases. In Fig. 6b, the strengths of the saturated specimens are significantly reduced, and most of them make the stress drop when the load reaches the peak strength. The yield platform near the peak stress is obviously reduced, which is related to the water weakening the bond between the materials during the plastic deformation process, and the frictional bearing capacity is reduced, which facilitates to the development of cracks. In addition, except for the specimen with 40 MPa confining pressure, the other specimens' peak strain all have varying degrees of reduction, especially the deformation of the elastic stage.

Table 4 shows the siltstone test results of triaxial compression in dry and saturated conditions, and the relevant mechanical parameters are also presented in the table. As shown in Table 4, in addition to the elastic modulus of saturated siltstone, the peak and residual stress, elastic modulus, and peak strain all increase with confining pressure increases. The residual strength has a great scatter. In order to better obtain the variation law of residual strength with confining pressure, more test results are needed to be provided. Compared with the dry specimen, the mechanical parameters of the saturated specimen are weakened under the same confining pressure. For example, the elastic modulus weakening coefficient which can be obtained by the ratio of saturated specimens' elastic modulus to dry specimens is 80.3% at 10 MPa, and the corresponding peak strain weakening coefficient (the ratio of saturated specimens' peak strain to dry specimens) is 87.7%. It shows that plastic deformation is more susceptible to water than elastic deformation in the pre-peak stage.

## Strength criterion

The Coulomb criterion has a clear physical background, that is, the shear strength is composed of the cohesion and internal friction of the rock materials. The expression of its principal stress form is

$$\sigma_s = Q + K\sigma_3 \tag{5}$$

where $\sigma_3$ is the minimum principal stress, $\sigma_s$ is the maximum axial stress, $Q$ is equivalent to the UCS, and $K$ is the influence coefficient of the confining pressure on the triaxial strength. Equation (5) indicates that the triaxial compression strength linearly increases with the confining pressure. However, the results of the conventional triaxial test on many rocks show that the strength curve is convex under confining pressure (Mogi 2007). When the confining pressure is zero, the strength curves of some rocks may be discontinuous, namely, the rock may exhibit axial splitting failure rather than shear failure under the low confining pressure.

There are various sizes of fissures and pores in the rock, and the cohesion and friction of rock cannot act at the same location simultaneously. The true cohesion of rock materials is

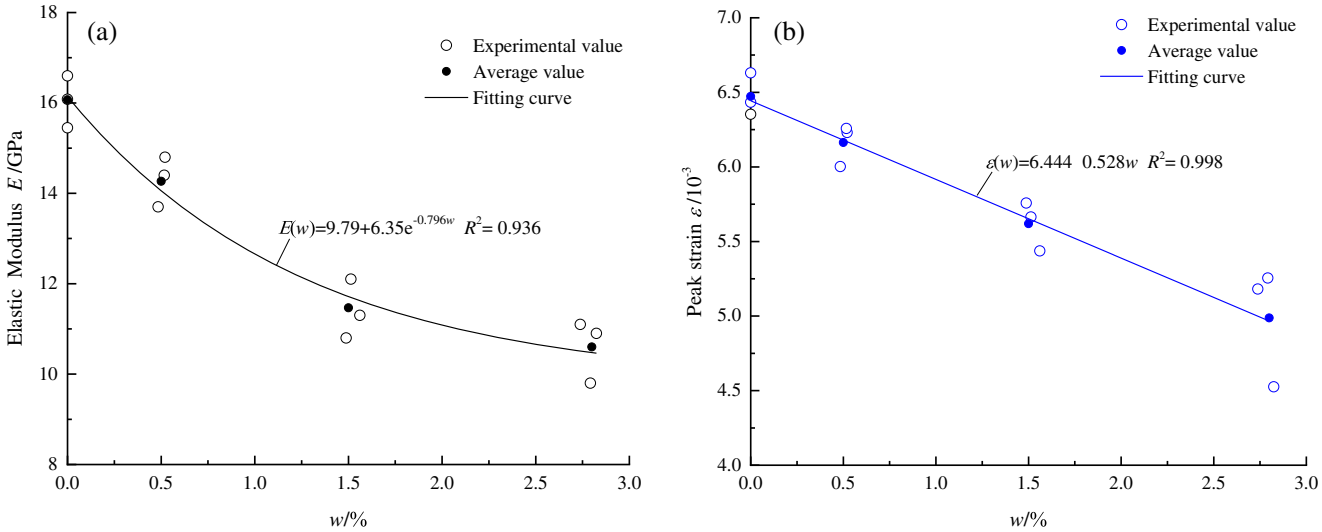


**Fig. 5** Variation of deformation parameters with water content for siltstone. **a** Elastic modulus. **b** Peak strain

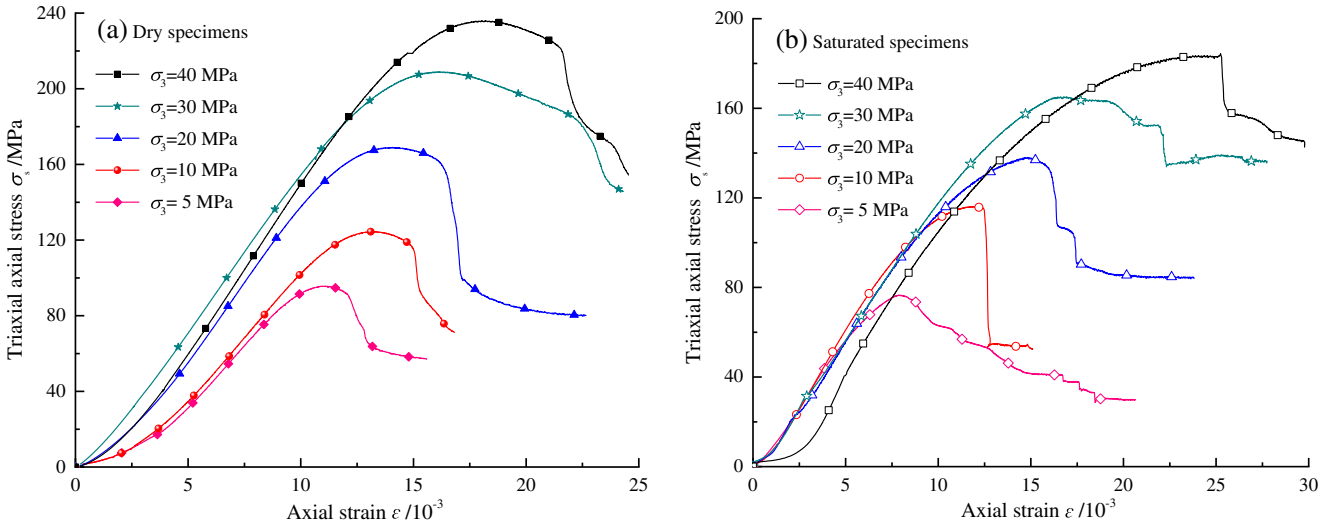


**Fig. 6** The triaxial compression stress-strain curves of siltstone in different conditions. **a** Dry condition. **b** Saturation condition

independent of confining pressure, and the internal friction increases with confining pressure or normal stress increases. Based on this view, You M. proposed an exponential strength criterion (You 2010)

$$\sigma_s - \sigma_3 = Q_\infty - (Q_\infty - Q_0)\exp\left[-\frac{(K_0-1)\sigma_3}{Q_\infty - Q_0}\right] \quad (6)$$

where $Q_0$ is the UCS; $Q_\infty$ is the limit value of differential principal stress when the confining pressure increases to infinite. $Q_\infty/2$ can be used as the maximum shear stress that rock can carry; $K_0$ is the initial rising rate of triaxial compression strength when confining pressure is zero, which corresponding friction angle can be used as the low estimation of the fracture friction angle (Li and You 2016). The result of fitting the test data of formula (6) is recorded as EX ($Q_0$, $Q_\infty$, $K_0$; $mf_E$), so the result of formula (5) is recorded as CO ($K$, $Q$; $mf_c$). The strength criterion fitting parameter is determined based on the least mean misfit ($mf$), which is slightly different from the result based on the least square method. The exponential strength criterion can better fit the test results than other conventional triaxial strength criteria and highlight the abnormal data points (You 2010, 2011).

## Triaxial compression strength and deformation test results

Figure 7 shows the strength varies with confining pressure of dry and saturated specimens. The fitting results of the exponential strength criterion are also shown in the figure. As shown in Fig. 7, the siltstone strength is significantly increased under the confining pressure. On the one hand, the failure of the specimen is related to the weak planes existing inside of it. The frictional bearing capacity of weak planes is improved with the confining pressure increases. When the slip resistance provided by the friction is greater than the shear stress caused

**Table 4** Physicomechanical parameters of rock specimens in dry and saturated conditions under triaxial compression

| Specimen no. | Density ($\rho$)/kg m$^{-3}$ | Water content ($w$)/% | Confining pressure ($\sigma_3$)/MPa | Peak stress ($\sigma_s$)/MPa | Residual stress ($\sigma_r$)/MPa | Elastic modluls ($E$)/GPa | Peak strain ($\varepsilon$)/10$^{-3}$ |
|---|---|---|---|---|---|---|---|
| AT1-1 | 2193.7 | 0 | 5 | 95.6 | 57.2 | 15.38 | 11.063 |
| AT1-2 | 2250.1 | 0 | 10 | 124.5 | 71.6 | 16.29 | 13.153 |
| AT1-3 | 2261.9 | 0 | 20 | 169.0 | 83.8 | 18.52 | 14.842 |
| AT1-4 | 2253.3 | 0 | 30 | 208.9 | 145.6 | 18.95 | 16.118 |
| AT1-5 | 2280.1 | 0 | 40 | 236.1 | 156.8 | 19.80 | 18.182 |
| AT2-1 | 2259.7 | 2.867 | 5 | 76.6 | 29.7 | 11.81 | 7.927 |
| AT2-2 | 2309.9 | 2.839 | 10 | 111.2 | 52.5 | 13.08 | 11.537 |
| AT2-3 | 2318.9 | 2.811 | 20 | 138.1 | 81.9 | 12.14 | 14.279 |
| AT2-4 | 2289.8 | 2.755 | 30 | 165.1 | 135.4 | 11.51 | 16.584 |
| AT2-5 | 2284.3 | 2.771 | 40 | 185.4 | 142.4 | 11.98 | 24.637 |

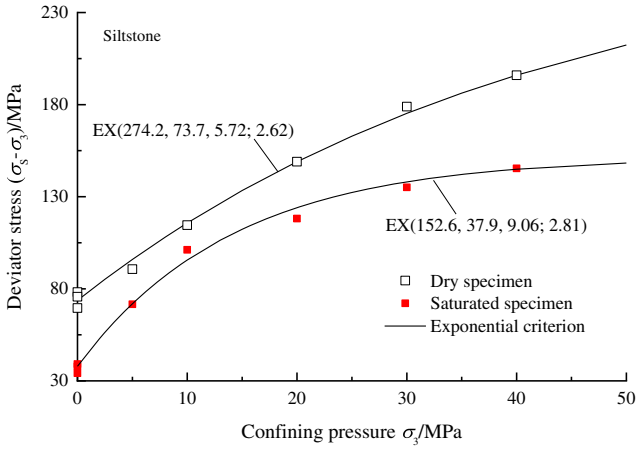


**Fig. 7** Strengths of siltstone specimens and fitting curves with the exponential criterion

by the axial loading, the weak plane slip is suppressed. In order to make it slip break, it is required to provide higher shear stress in the axial direction; therefore, the triaxial strength is improved under confining pressure. On the other hand, the presence of water changes the distribution of fissures and defects contained in the specimen, so the influence of confining pressure is different.

Under the low confining pressure, the distribution of fissures in the specimen can affect the strength of the rock. The strength of siltstone varies linearly within 10 MPa and satisfies the Coulomb criterion, but the cohesion and friction angle determined by this criterion are not true parameters of rock materials, which is related to the fissures with a specific angle inside a specimen. The differential stress varies nonlinearly in the range of the test. The dry specimens' strength is obviously higher than saturated specimens under the same confining pressure. When the confining pressure is less than 20 MPa, the strength of the specimen increases rapidly with confining pressure. After 20 MPa, the strength increases tend to be flattened. The trend of strength changes can be determined with the exponential criterion under the confining pressure. In Fig. 7, the strength of the saturated specimens tends to be constant when the confining pressure increases to infinite. The difference of strength with dry specimen tends to reach 121 MPa, which is determined using the exponential criterion. The shear strength of siltstone reduces by 60 MPa due to water-weakened effect and the strength loss rate is about 21.9%. Compared with the UCS loss rate of 50.1%, it indicated that the effect of confining pressure inhibits weakening of water on strength, so the water-rich rock engineer should be timely supported after excavation.

Table 5 shows the fitting results of the conventional triaxial strength in two conditions based on the least absolute deviation using the Coulomb and exponential criteria. As shown in Table 5, the UCS obtained with Coulomb criterion is higher than the average value of test results and the deviation is large, and the fitting result of the exponential criterion is equivalent to the experimental result. Based on the fitting deviation, the fitting result of the exponential criterion is obviously better than the Coulomb criterion.

The peak strain and elastic modulus variation with confining pressure is presented in Fig. 8. The elastic modulus and peak strain are positively correlated with the confining pressure in these two conditions. The elastic modulus increases slightly as the confining pressure increases, and the elastic modulus of saturated specimens are significantly lower than the dry specimens. In this case, the influence of water-weakening effect on the elastic modulus is greater than the confining pressure. Except for the specimen of 40 MPa, the peak strain of the saturated specimens is slightly smaller than dry specimen under the same confining pressure. The influence of confining pressure on the peak strain is greater than that of water, which is exactly opposite to the result of the elastic modulus.

## Analysis of microscopic damage mechanism

### Effect of water content on microstructure

In order to reveal the changes of microstructure and mineral morphology after encountering water, the SEM Quanta250 was used to measure the microscopic morphology features of siltstone. Four cubic specimens with a side length of 10 mm were cut and polished from the same dried sample, and then they were subjected to different water content, respectively.

Figure 9 shows the SEM images of siltstone with different water content. A small number of initial microcracks and micropores in the dry specimens and the mineral granules are

**Table 5** Conventional triaxial strength fitting results with two kinds of strength criteria for siltstone in the dry and saturated condition.

| Rock types | Moisture conditions | Average UCS/MPa | Coulomb criterion | | | Exponential criterion | | | |
|---|---|---|---|---|---|---|---|---|---|
| | | | $K$ | $Q$/MPa | $mf_C$/MPa | $K_0$ | $Q_\infty$/MPa | $Q_0$/MPa | $mf_E$/MPa |
| Siltstone | Dry | 75.2 | 3.19 | 77.5 | 5.11 | 5.72 | 274.2 | 73.7 | 2.62 |
| | Saturated | 37.1 | 2.82 | 48.3 | 12.37 | 9.06 | 152.6 | 37.9 | 2.81 |

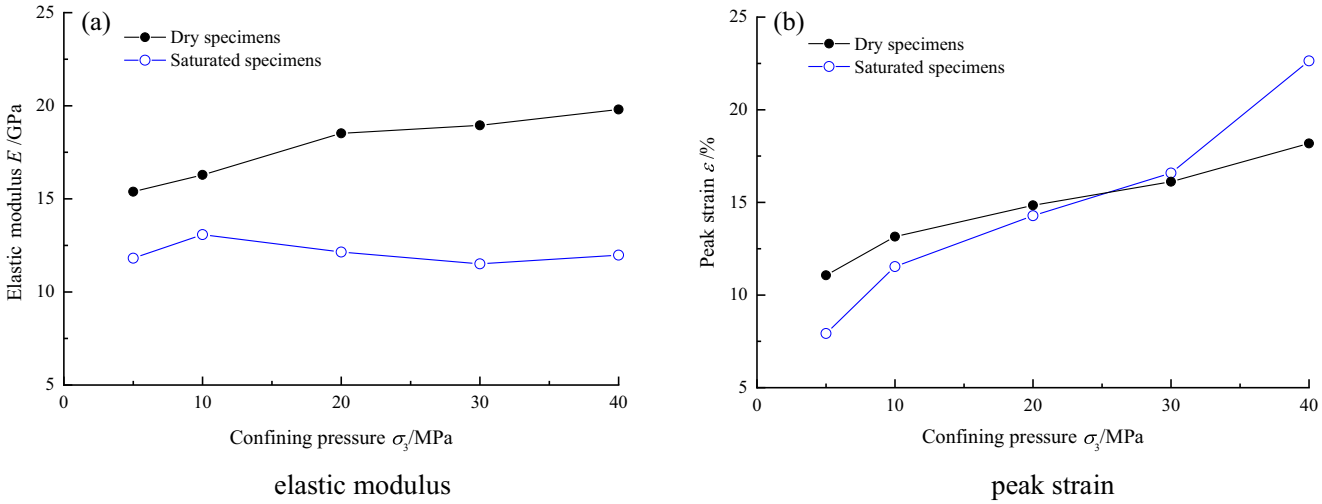


**Fig. 8** Variation of deformation parameters of siltstone with confining pressure in the dry and saturated condition. **a** Elastic modulus. **b** Peak strain

dense and intact. The quartz and feldspar grains are mainly surrounded by clay minerals (Fig. 9a). In the initial water absorption stage, new microcracks are sprouted and the initial microcracks begin to develop, the cement between granules begins to decrease, and the intact particles gradually dissolve and became loose (Fig. 9b). As the water content continues to increase, in Fig. 9c, most of the micropores are connected to form larger pores, and more microcracks sprout and develop. Lots of loose small particles appear. The contact mode between granules changes from face-to-face to point-to-surface.

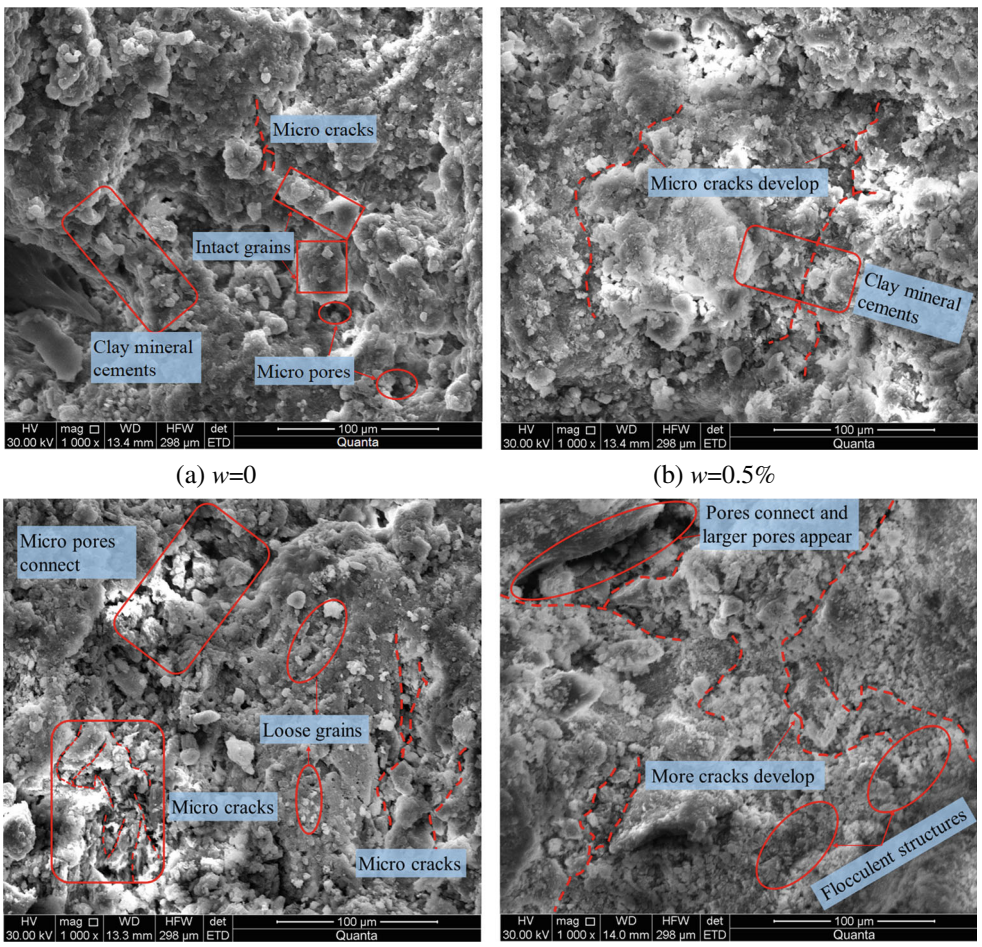


**Fig. 9** Scanning Electron Microscope photomicrographs of siltstone specimens in different water content. **a** $w = 0$. **b** $w = 0.5\%$. **c** $w = 1.5\%$. **d** $w = 2.8\%$

In Fig. 9d, the specimen reaches saturation state, both the size and number of cracks are significantly increased and the open cracks appear. The clay minerals are hydrolyzed and formed irregular flocculent structure. The intergranular connections become looser and the structure becomes porous. These phenomena indicate that when siltstone specimen is saturated, the cementation ability between some mineral granules is weakened, even lost, which result in the decrease of macroscopic cohesion.

The degradation of macroscopic mechanical characteristics of siltstone after encountering water is closely associated with the change of its microstructure.

## Microscopic analysis of water absorption-weakening damage

The mechanical characteristics of rock materials are completely different due to the difference of mineral composition and cementation type. The weakened effect of water on rocks is related to clay minerals and porosity. A series of chemical and physical interactions between hydrophilic mineral materials lead to weakening damage in siltstone after water absorption, which affects the mechanical parameters such as strength and deformation.

Figure 10 presents the schematic diagram of the specimen water absorption process. In Fig. 10a, the pore structure and the distribution of clay minerals are abstracted from the SEM results of the dry specimen (Fig. 9a). The water molecules flow into the sample under the driving force of capillary force, surface adsorption force, and osmotic pressure, and a bound water film is formed on the particle surface to weaken the frictional effect between the particles. Subsequently, the large pores and open cracks in the specimen are quickly filled with water, and the clay minerals in the large pores absorb water and expand. At this stage, the water content of the specimens increases rapidly (Fig. 10a). As the water absorption time increases, the water molecules gradually enter the micropores and cracks, the soluble clay mineral dissolved, and the porosity gradually increases. Finally, the specimen reaches a saturation state (Fig. 10c).

In Fig. 10b, the gas in the space between intergranular pores constantly replaced by water with the soaking time increases. From a microscopic point, a thin liquid film is formed and then the liquid bridge occurs between the mineral grains. Considering the liquid bridge force acts as a part of cohesion between the particles, it is significantly affected by the increase of water content (Matthewson 1988; Soulié et al. 2006; Tsunazawa et al. 2016). To elaborate on the influence of water on the particle cohesion, a simplified liquid bridge model is presented in Fig. 11. The liquid bridge force includes the axial component of the surface tension and the capillary force, assuming that two particles have the same radius and the liquid bridge between the particles is cylindrical, so it can be expressed as a function of separation distance $D$ between two spheres (Olivier et al. 2000; Vincent et al. 2009):

$$F_{\text{cap}} = 2\pi\sigma R\cos\theta\exp(-D/\lambda) \tag{7}$$

where $\sigma$ is the surface tension; $R$ is the radius of the sphere; $\theta$ is the contact angle; λ can be obtained as a function of bridge volume $V$ and the sphere radius:

$$\lambda = \mathrm{c}(V/R)^{1/2} \tag{8}$$

where c is a constant. Equation (7) is suit for the polydisperse particle capillary force by setting $c = 0.9$.

When the two particles are in contact ($D = 0$), the liquid bridge force reaches a maximum value $2\pi\sigma R\cos\theta$, and then it falls off exponentially as the separation distance $D$. The liquid bridge is stable as long as $D < D_{\max}$ which is critical separation distance, if beyond the critical distance, it breaks into two parts. The $D_{\max}$ can be defined as (Lian et al. 1993)

$$D_{\max} = \left(1 + \frac{\theta}{2}\right)V^{1/3} \tag{9}$$

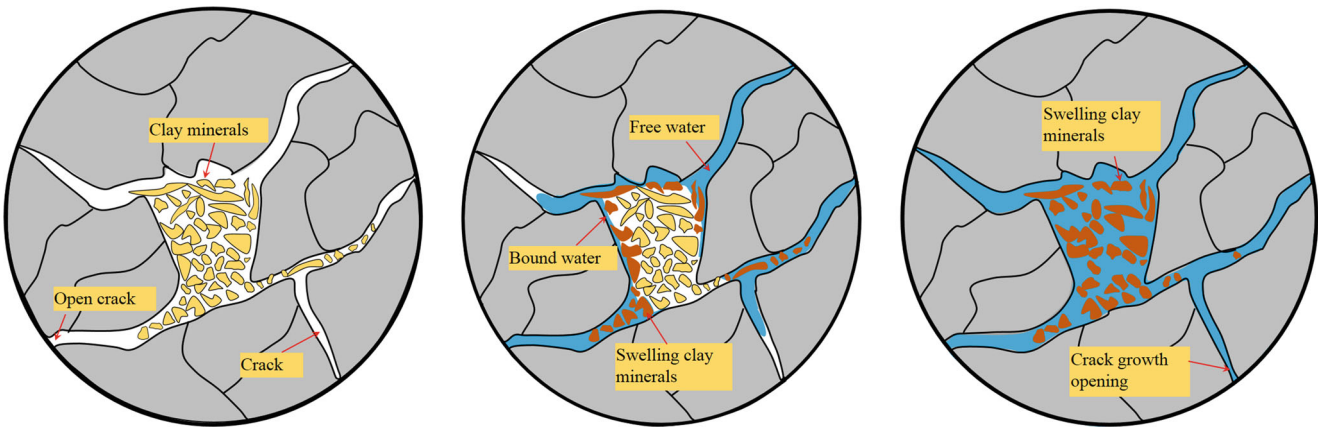


(a) Dry state (b) Absorbing water state (c) Saturation state

**Fig. 10** Diagram of the water absorption process of siltstone. **a** Dry state. **b** Water absorption state. **c** Saturation state

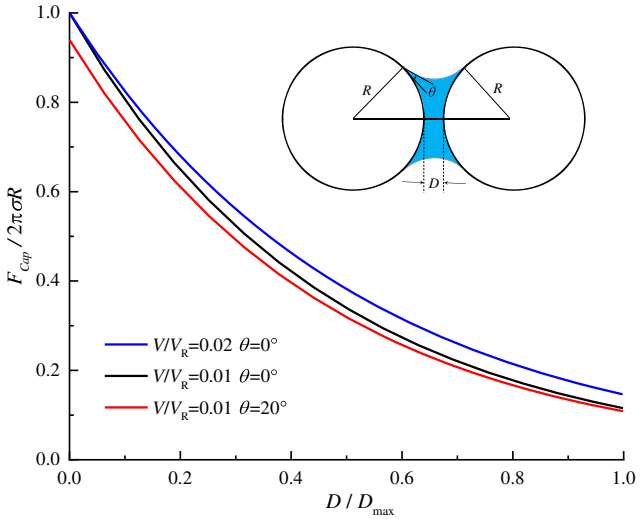


**Fig. 11** Relationship of normalized liquid-bridge force and separation distance with different values of liquid volume $V$ and contact angle $\theta$. Inset: a simplified liquid bridge model

It is obvious that the critical distance $D_{max}$ is related to liquid volume $V$ and contact angle $\theta$.

Figure 11 shows the relationship of the liquid bridge force $F_{cap}$ with particle distance $D$. The force $F_{cap}$ and distance $D$ are normalized by $2\pi\sigma R$ and $D_{max}$, respectively. Volume $V$ is normalized by the particle volume $V_R$. At a specific volume, when the spheres move away from each other, the liquid bridge force decreases. The force $F_{cap}$ is much more affected by distance $D$ than volume $V$ and contact angle $\theta$, and the increase of $D$ and $\theta$ makes the force between the particles decrease, while the volume increase causes the liquid bridge force to increase slightly.

During the water absorption process, the space between adjacent mineral particles becomes a region with a high ion concentration according to the electrical double-layer repulsion, and the difference of ion concentration with the surrounding water drives the water molecules into the interspace, increasing the distance between particles (Schult and Shi 1997). On the other hand, the dissolution of the soluble material around the particles also causes the distance between the particles to become larger. The solvation forces of soluble particles lead to loss of rock skeleton material and reduction of van der Waals force between particles (Jia et al. 2018). In addition, the volume and the contact angle increase when water content increases, but the influence of the distance and contact angle on the force far exceeds the volume, which results in the decrease of the liquid bridge force. Finally, the cohesion of interparticle is reduced.

In Fig. 10c, the free water fills the crack tip region of the saturated specimen. According to the XRD test results, the

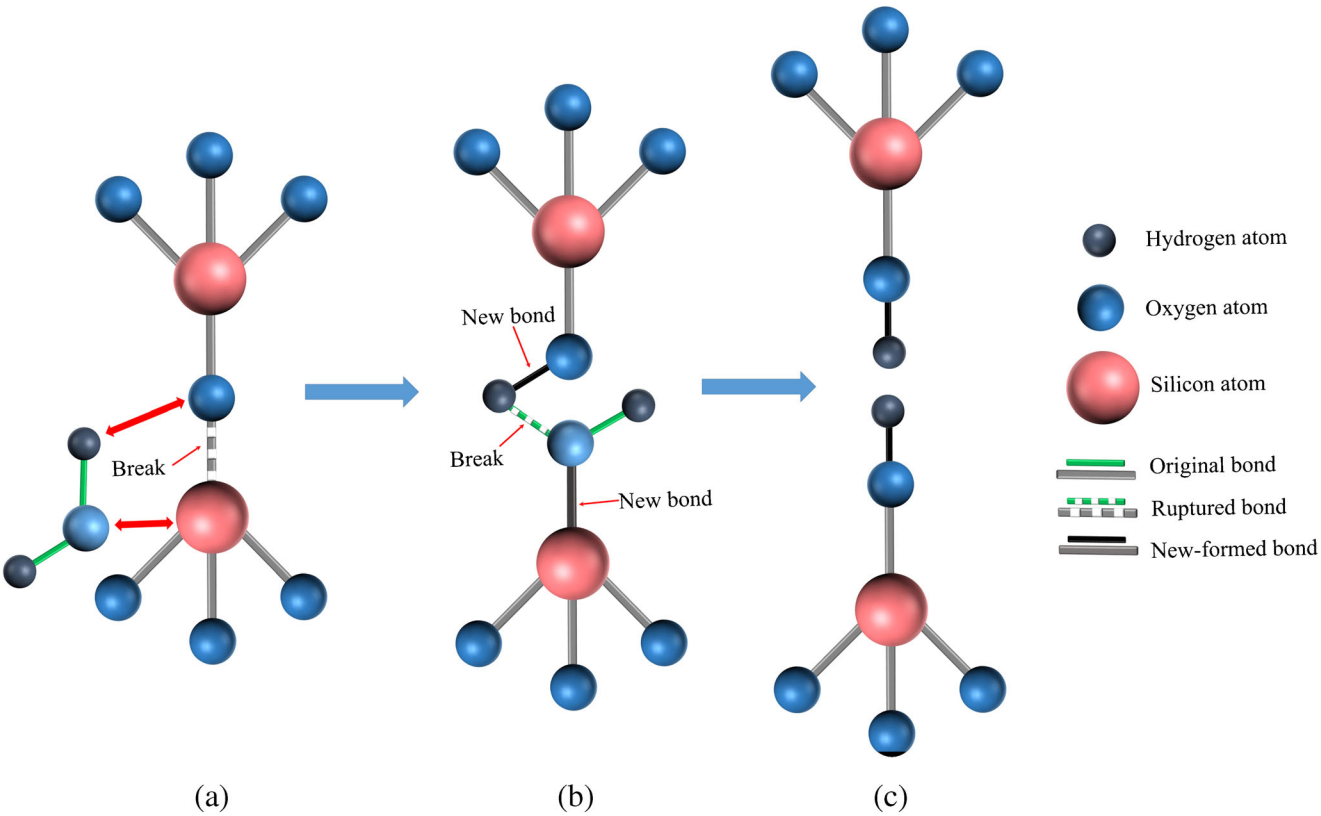


**Fig. 12** Diagram of the hydrolysis reaction between a Si–O–Si bond and a water molecule at the crack tip (modified after Michalske and Freiman 1982 and Zhou et al. 2018). (a) Si–O bond encounters water molecule then it's ruptured. (b) The O–H bond is ruptured and two new bonds are formed. (c) Two Si–O–H groups are formed.

content of quartz in this siltstone is as high as 71%. For rocks with abundant quartz mineral, water molecules ($H_2O$) can react with quartz ($SiO_2$) to cause hydrolysis damage even in a pure water environment. A simplified model of the chemical reaction mechanism is shown in Fig. 12 (Michalske and Freiman 1982). A general expression for a Si–O bond reacting with $H_2O$ is presented by (Atkinson and Meredith 1987; Freiman 1984):

$$\mathrm{H{-}O{-}H} + [\equiv \mathrm{Si{-}O{-}Si} \equiv] \rightleftharpoons [\equiv \mathrm{Si{-}OH} \cdot \mathrm{HO{-}Si} \equiv] \rightleftharpoons 2[\equiv \mathrm{Si{-}OH}] \quad (10)$$

The strong Si–O bonds were hydrolyzed to weaker hydrogen bond hydroxyl groups linking the silicon atoms in Eq. (10). The increase of hydroxyl ion concentration can accelerate the cracking speed of microcracks under stress.

After the specimen absorbs water, the hydrolysis of quartz mineral produces stress corrosion and an intensive microcrack zone was formed in the crack tip region. The development of subcritical crack is related to the water content and the diffusion rate of water molecules. During the loading process, the presence of water lowers the stress threshold of microcrack development, resulting in the microcrack of the specimen to develop at a lower stress level (Hadizadeh and Law 1991). In addition, the growth rate of subcritical crack in a humid environment is faster than that in a dry state (Atkinson 1979; Yoshitaka et al. 2011). On the other hand, the siltstone has a high clay mineral content, and the sum of illite and kaolinite is as high as 14.9%. When kaolinite encounters water, the bound water film of granules surface becomes thicker, which leads to expand of granule volume and the cohesion between granules reduces. The physicochemical reaction of illite with water increases the volume by 50~60% (Zhu 1996). The expansion force generated by interlayer or intergranular expansion promotes the growth of initial cracks and the formation of new cracks, which reduces the resistance to deformation of the material.

In summary, the weakening damage of siltstone in this paper is mainly caused by the physicochemical interaction between mineral components and water. As the water content increases, the microscopic damage continues to develop. Eventually, the accumulation of microscopic damage leads to the weakening of macroscopic mechanical properties.

## Conclusion

The mechanical properties of siltstone specimens in different water content conditions were studied in this paper. Uniaxial and triaxial compression tests were implemented to investigate the weakening of macroscopic mechanical properties. The SEM test was used to analyze the change of microstructure. As to the analysis above, the following conclusions are reached:

The water content increases nonlinearly with water absorption time and finally tends to be about 2.8% in saturation. The UCS, elastic modulus, and peak strain all decrease as the water content increases. The difference is that the UCS and elastic modulus vary nonlinearly with water content, and their relationships can be described with an exponential equation, while the relationship of water content and peak strain is linear in the range of the test. When the specimen reached saturation state, its UCS loss rate reaches 50.1%.

For the triaxial compression stress-strain curve, the plastic deformation near the peak stress of the saturated specimen is smaller than that of the dry specimen under the same confining pressure. The specimen strength is nonlinearly increased when the confining pressure increases in dry and saturated condition, which can be described by exponential strength criterion. The peak strain is positively correlated with confining pressure and the influence of confining pressure on peak strain is greater than that of water. Compared with the dry specimens, the shear strength of saturated specimens eventually reduces by 60 MPa under confining pressure, and the strength loss rate is about 21.9%. Compared with the UCS loss rate of 50.1%, it indicated that the effect of confining pressure inhibits weakening of water on strength.

The weakening damage of siltstone is mainly due to the physicochemical reaction between minerals and water. As the water content increases, the SEM results show that the size and number of microcracks increase, the structure becomes loose, and the microscopic damage accumulates. The hydration of clay minerals reduces the local cohesion of the specimen, and the hydrolysis of quartz minerals in crack tip region promotes subcritical crack growth, which collaboratively leads to the reduction in the bearing capacity of saturated specimen.

**Funding information** This work was supported by the National Key R&D Program of China (Grant no. 2016YFC0401802), the State Key Program of National Natural Science of China (Grant no. 51539002), the National Natural Science Foundation of China (Grant no. 51779249), and the Natural Science Foundation of Hubei Province (Grant no. 2018CFB632).

## References

Atkinson BK (1979) A fracture mechanics study of subcritical tensile cracking of quartz in wet environments. Pure Appl Geophys 117: 1011–1024

Atkinson BK, Meredith PG (1987) The theory of subcritical crack growth with applications to minerals and rocks. Academic Press, London, Fracture Mechanics of Rocks, pp 111–166

Bagheripour MH, Rahgozar R, Pashnesaz H et al (2011) A complement to Hoek-Brown failure criterion for strength prediction in anisotropic rock. Geomech Geoeng 3:61–81

Baud P, Zhu W, Wong TF (2000) Failure mode and weakening effect of water on sandstone. J Geophys Res 105(B7):16371–16389

Bian K, Liu J, Liu ZP et al (2019) Mechanism of large deformation in soft rock tunnel: a case study of Huangjiazhai Tunnel. Bull Eng Geol Environ 78:431–444

Bian K, Liu J, Zhang W et al (2019) Mechanical behavior and damage constitutive model of rock subjected to water-weakening effect and uniaxial loading. Rock Mech Rock Eng 52:97–106

Burshtein LS (1969) Effect of moisture on the strength and deformability of sandstone. J Min Sci 5(5):573–576

Chang C, Haimson B (2007) Effect of fluid pressure on rock compressive failure in a nearly impermeable crystalline rock: implication on the mechanism of borehole breakouts. Eng Geol 89:230–242

Chen GQ, Li TB, Wang W et al (2019) Weakening effects of the presence of water on the brittleness of hard sandstone. Bull Eng Geol Environ 78:1471–1483

Chinese National Standard SL264–2001 (2001) Specifications for rock tests in water conservancy and hydroelectric engineering. The National Ministry of Water Resources of the People's Republic of China, Beijing (in Chinese)

Erguler ZA, Ulusay R (2009) Water-induced variations in mechanical properties of clay-bearing rocks. Int J Rock Mech Min Sci 46(2): 355–370

Freiman SW (1984) Effects of chemical environments on slow crack growth in glasses and ceramics. J Geophys Res Solid Earth 89: 4072–4076

Hadizadeh J, Law RD (1991) Water-weakening of sandstone and quartzite deformed at various stress and strain rates. Int J Rock Mech Min Sci 28(5):431–439

Haimson B (2006) True triaxial stresses and the brittle fracture of rock. Pure Appl Geophys 163:1101–1130

Hashiba K, Fukui K (2015) Effect of water on the deformation and failure of rock in uniaxial tension. Rock Mech Rock Eng 48: 1751–1761

Hawkins AB, Mcconnell BJ (1992) Sensitivity of sandstone strength and deformability to changes in moisture content. Q J Eng Geol Hydrogeol 25(2):115–130

Hoek E (1990) Estimating Mohr-Coulomb friction and cohesion values from Hoek–Brown failure criterion. Int J Rock Mech Min Sci 27: 227–229

Hu DW, Zhang F, Shao JF et al (2014) Influences of mineralogy and water content on the mechanical properties of argillite. Rock Mech Rock Eng 47:157–166

Hudson JA, Harrison JP (2000) Engineering rock mechanics-an introduction to the principles. Elsevier, New York

ISRM (1978) Suggested methods for determining the strength of rock materials in triaxial compression. Int J Rock Mech Min Sci Geomech Abstr 15:99–100

Iverson RM (2000) Landslide triggering by rain infiltration. Water Resour Res 36(7):1897–1910

Jia HL, Wang T, Xiang W et al (2018) Influence of water content on the physical and mechanical behavior of argillaceous siltstone and some microscopic explanations. Chin J Rock Mech Eng 37(7):1618–1628

Li BY, You MQ (2016) Study on nonlinear strength property of rocks with cohesion and friction using the exponential criterion. Chin J Rock Mech Eng 35(10):1945–1953

Li D, Wong LNY, Liu G et al (2012) Influence of water content and anisotropy on the strength and deformability of low porosity metasedimentary rocks under triaxial compression. Eng Geol 126: 46–66

Lian G, Thornton C, Adams MJ (1993) A theoretical study of the liquid bridge forces between two rigid spheres. J Colloid Interface Sci 161: 138–147

Liu TY, Cao P (2016) Testing study of subcritical crack growth mechanism during water-rock interaction. Geotech Geol Eng 34:923–929

Lu YL, Wang LG, Sun XK et al (2017) Experimental study of the influence of water and temperature on the mechanical behavior of mudstone and sandstone. Bull Eng Geol Environ 76:645–660

Matthewson MJ (1988) Adhesion of spheres by thin liquid films. Philos Mag 57:207–216

Michalske TA, Freiman SW (1982) A molecular interpretation of stress corrosion in silica. Nature 295:511–512

Mogi K (2007) Experimental rock mechanics. Taylor and Francis, London, pp 32–48

Olivier P, Pascal M, Xavier C (2000) Liquid bridge between two moving spheres: an experimental study of viscosity effects. J Colloid Interface Sci 231:26–31

Roy DG, Singh TN, Kodikara J et al (2017) Effect of water saturation on the fracture and mechanical properties of sedimentary rocks. Rock Mech Rock Eng 50(10):2585–2600

Schult A, Shi G (1997) Hydration swelling of crystalline rocks. Geophys J Int 131(1):179–186

Sofianos AI, Nomikos PP (2006) Equivalent Mohr-Coulomb and generalized Hoek–Brown strength parameters for supported axisymmetric tunnels in plastic or brittle rock. Int J Rock Mech Min Sci 43: 683–704

Soulié F, Cherblanc F, Youssoufi MS et al (2006) Influence of liquid bridges on the mechanical behavior of polydisperse granular materials. Int J Numer Anal Methods Geomech 30: 213–228

Tang SB (2018) The effects of water on the strength of black sandstone in a brittle regime. Eng Geol 239:167–178

Torres-Suareza MC, Alarcon-Guzman A, Moya RD (2014) Effects of loading-unloading and wetting-drying cycles on geomechanical behaviors of mudrocks in the Colombian Andes. J Rock Mech Geotech Eng 6:257–268

Tsunazawa Y, Fujihashi D, Fukui S et al (2016) Contact force model including the liquid-bridge force for wet-particle simulation using the discrete element method. Adv Powder Technol 27:652–660

Vásárhelyi B, Ván P (2006) Influence of water content on the strength of the rock. Eng Geol 84:70–74

Verstrynge E, Adriaens R, Elsen J et al (2014) Multi-scale analysis on the influence of moisture on the mechanical behavior of ferruginous sandstone. Constr Build Mater 54:78–90

Vincent R, Youssoufi MS, Emilien A et al (2009) Force transmission in dry and wet granular media. Powder Technol 190: 258–263

Wong LNY, Varun M, Liu G (2016) Water effects on rock strength and stiffness degradation. Acta Geotech 11:713–737

Wu QH, Weng L, Zhao YL et al (2019) On the tensile mechanical characteristics of fine-grained granite after heating/cooling treatments with different cooling rates. Eng Geol 253:94–110

Yang SQ, Jing HW, Wang SY (2012) Experimental investigation on the strength, deformability, failure behavior and acoustic emission locations of red sandstone under triaxial compression. Rock Mech Rock Eng 45:583–606

Yao QL, Li XH, Zhou J et al (2015) Experimental study of strength characteristics of coal specimens after water intrusion. Arab J Geosci 8:6779–6789

Yoshitaka N, Kazuya M, Tetsuro Y et al (2011) Effects of humidity and temperature on subcritical crack growth in sandstone. Int J Solids Struct 48:1130–1140

You MQ (2010) Three independent parameters to describe conventional triaxial compressive strength of intact rocks. J Rock Mech Geotech Eng 2(4):350–356

You MQ (2011) Comparison of the accuracy of some conventional triaxial strength criteria for intact rock. Int J Rock Mech Min Sci 48:852–863

Zhang ZH, Jiang QH, Zhou CB et al (2014) Strength and failure characteristics of Jurassic red-bed sandstone under cyclic wetting-drying conditions. Geophys J Int 198:1034–1044

Zhou ZL, Cai X, Ma D et al (2018) Effects of water content on fracture and mechanical behavior of sandstone with a low clay mineral content. Eng Fract Mech 193:47–65

Zhu XJ (1996) Characteristics of soft rocks interacting with water. Sci Technol Min 4(3):46–50